

Reorganization of coherent structures downstream a circular cylinder located between two parallel walls

Férid REHIMI ^{*1}, Fethi ALOUI ^{2,3}, and Sassi BEN NASRALLAH ¹

¹ *Université de Monastir, École Nationale d'Ingénieurs de Monastir, Laboratoire LESTE, Avenue Ibn El Jazzar 5019 - Monastir, Tunisie*

² *Université de Nantes, Faculté des Sciences et des Techniques, Département de Physique, 2, rue de la Houssinière BP 92206 - 44322 Nantes Cedex 03, France*

³ *GEPEA, CNRS - UMR 6144, École des Mines de Nantes, DSEE 4, rue Alfred KASTLER - BP 20722 - 44307 Nantes Cedex 03, France*

* Email: *rehimi_f@yahoo.fr*

ABSTRACT

Experiments were performed at low Reynolds numbers in the range $75 \leq Re \leq 275$ in the wake of a circular cylinder of d_c diameter placed symmetrically between two parallel walls of H height. 2D2C particle image velocimetry (PIV) was used to investigate the flow downstream the cylinder. In the unsteady flow regime downstream the cylinder, the detached primary vortices (Pi) interact with walls generating secondary ones (Pi') and modify the cylinder wake dynamic. The kinematical properties (advection velocity, circulation, rotation kinetic energy, etc.) of the generated secondary vortices are studied and compared with the primary ones in order to show how the walls influence the von Kármán vortex street. The authors propose here a relation between the circulations and kinetic energies of primary and secondary vortices.

KEYWORDS: Confined cylinder wake, PIV measurements, von Kármán vortices, Coherent structures, Γ_2 criterion, Wall-vortex interaction.

NOMENCLATURE

a, b	Tunnel section dimensions (m)
Cir	Vortex circulation (m^2/s)
d_c	Cylinder diameter (m)
H	Tunnel height (m)
Re	Reynolds number (dimensionless)
Sv	Vortex area (m^2)
r	Confinement rate (dimensionless)
T	Duration of a pair of von Kármán vortices (s^{-1})
U	Velocity (m/s)

Greek letters

Γ_2	Dimensionless criterion
Δ	Distance between the cylinder and the lower wall
γ	Gap parameter
ν	Kinematic viscosity (m^2/s)

Subscripts

max	Maximum
turb	Turbulent
adv	Advection
c	With reference to the cylinder

1. INTRODUCTION

The flow around a circular cylinder placed between two parallel walls has received less attention than the case of the non confined cylinder. Few works were dedicated to the confined cylinder case.

Coutanceau and Bouard (1977) have studied experimentally the flow of a uniform moving confined cylinder. Zovatto and Pedrizzetti (2001) have studied numerically the confined cylinder case by putting attention to the additional control parameters of the flow which are the gap parameter

$\gamma = \Delta/d_c$ (Δ is the distance between the cylinder and the nearest wall, and d_c the cylinder diameter) and blockage ratio called also confinement rate defined as $r = d_c/H$ (H is the distance separating the two walls). Their attentions were focused of the influence of the gap parameter on the von Kármán instability appearance and on the lift and drag coefficients calculated on the cylinder. Guerrouache (2000) has studied the flow past a circular cylinder placed symmetrically between two parallel walls (i.e.: $r = 1/3$ and $\gamma = 1$). In his study, he shows that the confinement affects the first instability by delaying its appearance to $Re \approx 100$ ($Re = U_{\max} d_c/\nu$, U_{\max} is the maximum velocity upstream the cylinder and ν is the kinematic viscosity) and by increasing the values of the Strouhal number in comparison with the non confined cylinder case. Yang et al. (1997) have studied both numerically and experimentally the influence of the confinement on the mass transfer at wall downstream a circular cylinder placed symmetrically between two parallel walls and they make the same conclusions about the delay in the appearance of the first instability and the increasing of the Strouhal number with the confinement rate. Sahin and Owens (2004) have showed by a stability analysis of the confined cylinder placed symmetrically between two parallel walls for different confinement rates that increasing the confinement rate delays the appearance of the first von Kármán instability which is a hopf bifurcation.

In this present work, the flow around a circular cylinder between two parallel walls is investigated experimentally. The experiments were conducted in a tunnel with a rectangular cross section. The measurements were done using Particle Image velocimetry (PIV). The Reynolds numbers covered in this work was in the range $5 \leq Re \leq 277$. PIV measurements were filtered using a proper orthogonal decomposition of the flow. The aim of this work is the study of the flow reorganization in the wake of a circular cylinder in the presence of confinement and the interaction of the generated coherent structures with walls.

2. EXPERIMENTAL FACILITY

The experiments were conducted in a hydraulic tunnel made up with transparent Plexiglas to permit visualizations. The tunnel has a rectangular cross-section of $0.3m \times 0.03m = (2a \times 2b)$, which was $3.3m$ in length (Fig.2a and 2b). It is fed by a tank where the water level is maintained constant by an over flow. At $L_b = 1.67m$ from the entry of the tunnel, a cylinder of $d_c = 10mm$ in diameter is

placed in the test section perpendicularly to the mean flow direction.

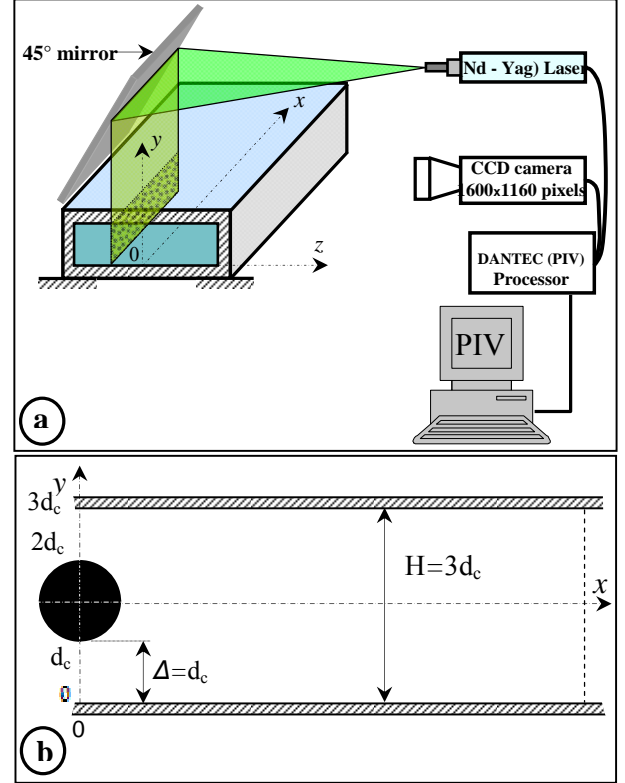


Figure 1: Sketch of the experimental setup:
a) 3D view; b) 2D view

The cylinder was placed symmetrically between the upper and the lower wall which give a gap parameter $\gamma = \Delta/d_c = 1$, where Δ is the distance between the cylinder and the nearest wall and the confinement ratio is $r = d_c/2b = 1/3$ (Fig.2.a). The fluid circuit is closed and the flow is assured by an isolated centrifugal pump. The mean flow velocity range studied in the tunnel section was in the range $2 \cdot 10^{-3} m/s$ to $18.5 \cdot 10^{-3} m/s$. The tunnel was constructed to satisfy the fact that the flow is laminar and developed for the range of Reynolds studied and the materials of the tunnel are non metallic to satisfy electrochemical measurements.

2.1 PIV measurements

The flow was seeded with a $50 \mu m$ polyamide spherical particles. The Laser pulses were generated using a pulsed Nd-Yag 15mJ Laser (type New wave Solo) and the images were captured by a CCD camera (type Dantec dynamics flow sense M2/E 8 bit) of $1600 \times 1186 \text{ pixel}^2$ of resolution with an objective Nikon (60mm). The whole system was driven by a Flow map processor (from Dantec Technology). Flow manager was used to calculate the velocity fields using an adaptative cross-correlation. The measurement position is

defined at $z=0$ with $0 \leq x \leq 8d_c$ and $0 \leq y \leq 3d_c$ (Fig.1.b). In the work presented by Rehimy et al. (2008) a second measurement position was taken and defined by and the second measurement position is defined by at $z=0$ with $9d_c \leq x \leq 18d_c$ and $0 \leq y \leq 3d_c$. The laser plane was horizontal and reflected vertically at $z=0$ using a Mirror laced at 45° from the horizontal plane. The camera was placed for the both cases in front of the reflected Laser plane (Fig.1.a). The physical field of view in the first position of measurements was $81.73 \times 60.59 \text{ mm}^2$. A mask was applied to retain only 30 mm in the y -direction from the 60.59 mm . The interrogation area was $32 \times 32 \text{ pixels}^2$ and an adaptative cross correlation was applied with an overlapping of 50%. The adaptative cross correlation was used with two passes and an initial interrogation region window size of $128 \times 128 \text{ pixels}^2$. The rejection criterion is based on the fact that if the velocity exceeds with 20% the neighbours it is replaced by the moving average of the neighbours. The spatial resolution obtained is $\Delta x = \Delta y = 0.85 \text{ mm}$ where the sampling rate was limited by the camera and was $fe = 15 \text{ Hz}$ for a duration of 25 s .

3. RESULTS AND DISCUSSIONS

3.1 Flow dynamic

Before placing the cylinder in the tunnel, it was necessary to verify that the flow was fully developed and laminar. Comparisons are made for the reason with those of Natarajan and Lakshmanan (1972). The experimental results are in agreement with the present work, see (Rehimy et al., 2008).

In the next step, the cylinder of $d_c = 10 \text{ mm}$ of diameter was placed at $L_b = 1.67 \text{ m}$ from the tunnel entry, perpendicularly to the mean flow direction, and positioned symmetrically between the upper and the lower wall. The Reynolds number was defined as $Re = U_{max} d_c / \nu$ where U_{max} is the maximum velocity value far upstream the cylinder and ν is the kinematic viscosity of the flow. The measurements downstream the cylinder, were taken in the plane ($z=0$). Theses measurements show a great similarity with the non confined cylinder case with some differences caused by the presence of walls confinement.

For $Re < Re_c \approx 108$, the flow is permanent, characterized by the preponderance of the viscous

effects and the presence of two contra-rotating steady vortices close to the cylinder(Fig.2). This flow regime is similar to that obtained for the non confined cylinder case for $Re < 47$.

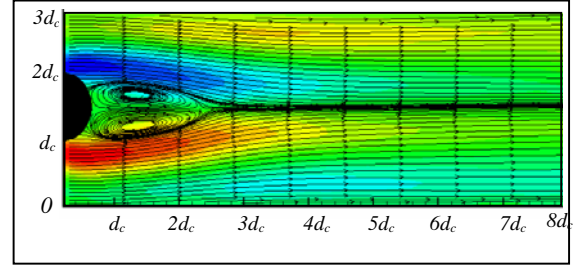


Figure 2. Vorticity and streamlines downstream the cylinder for $Re=100$

The critical Reynolds number was found to be about $Re_c \approx 108$ and can be estimated by observing the mean recirculation region L_r downstream the cylinder with Re (Rehimy et al., 2008). The value of the critical Reynolds number found was in good agreement with the numerical simulations of Carte et al.(1995), Guerrouache (2000) and the stability analysis of Sahin and Owens (2004). The mean recirculation region in the confined case is larger than the non confined case. The blocking effect of the walls tends to minimize and amortize fluctuations developing in the y -axis direction by elongating the mean recirculation region. This blocking effect of the walls delay the apparition of the first von Kármán instability appearing for the non confined case at $Re \approx 47$ (Williamson, 1989).

When $Re \geq Re_c$, the wake become unstable, begins to oscillate and we assist to the appearance of vortex pairs detaching alternately from each side of the cylinder and similar to the von Kármán vortex street found in the non confined case. The figure 3 represents successive snapshot maps of Γ_2 criterion (Graftieaux et al., 2001) where only the values of $|\Gamma_2| > \frac{2}{\pi}$ are represented. We remember

here the Γ_2 criterion is defined as:

$$\Gamma_2(P) = \frac{1}{S} \int_{M \in S} \frac{(\mathbf{PM} \wedge (\mathbf{U}(M) - \tilde{\mathbf{U}}(P))) \cdot \mathbf{e}_z}{\|\mathbf{PM}\| \cdot \|\mathbf{U}(M) - \tilde{\mathbf{U}}(P)\|} dS \quad (1)$$

where $\tilde{\mathbf{U}}(P) = \frac{1}{S} \int_{M' \in S} \mathbf{U}(M') dS$; \mathbf{e}_z is a unit vector

perpendicular to the velocity map; P is the point where the criterion is calculated, and S is a local surface surrounding the point P . The local surface S can be chosen circular or rectangular. For a large size of S , the small scales in the flow are filtered, so S should be as small as possible. The

size of S retained in our case is $S = 9 \Delta x \Delta y$. In the case of vector map with moderated resolution, the maximum of Γ_2 is not a point but a quasi-circular region.

By referring to the snapshots in the figure 3, we notice that the essential difference observed between confined and non confined cylinder case is that when a von Kármán vortex (P_1) (resp. (P_2)) (Fig.3.a) is detached from the lower (resp. upper) side behind the cylinder, the wall tends to oppose this vorticity created by generating at wall a vortex (P_1') (resp. (P_2')) with opposite sign vorticity which is advected downstream the cylinder at wall. More details about wall-vortex interactions can be found in the work of Escriva (1999). This interaction pushes the vortex (P_1) (resp. (P_2)) in the y-axis direction which crosses the tunnel to stabilize in the upper (resp. lower) wall. Before stabilizing in the upper (resp. lower) wall, the vortex (P_1) (resp. (P_2)) coalesce with a vortex same sign (P_2') (resp. (P_1')). Two principal differences in comparison with the non confined cylinder case; the first is that positive vortices (in term of rotation direction) are rolling on the upper side contrarily to the non confined case. The second difference is that the wavelength of the vortices in the second measurement position was $\Lambda \approx 3d_c$ for all the range of Reynolds studied and not about $4-5d_c$ as in the non confined case (Williamson, 1996). It should be also noticed that the vertical space between the vortex centers is about $1d_c$. In this regime, measurements of local axial or normal velocity show that the flow is characterized by a quasi-sinusoidal regime corresponding to the von Kármán vortices detachments. Nevertheless, for $Re \geq 194$, the von Kármán frequency persists but we assist to the apparition of a low frequency perturbation which can be due to the presence of three-dimensional perturbations in the flow.

The Strouhal number defined as $St = f_s d_c / U_{max}$ and obtained from both PIV measurements is found to be larger than 0.2 found in the non confined case and these results are in concordance with the numerical simulations of Carte et al. (1995), Guerrouache (2000), Sahin et Owens (2004) and both numerical and experimental results of Yang et al. (1997). The confinement rate increases the values of the Strouhal number for a given Reynolds number (Fig. 4).

The analysis of the PIV results using Γ_2 criterion permit to follow the axial positions of the vortices type (P_i) and (P_i') at different times (Fig. 3.) permit to calculate their advection velocity U_{ad} at different Reynolds.

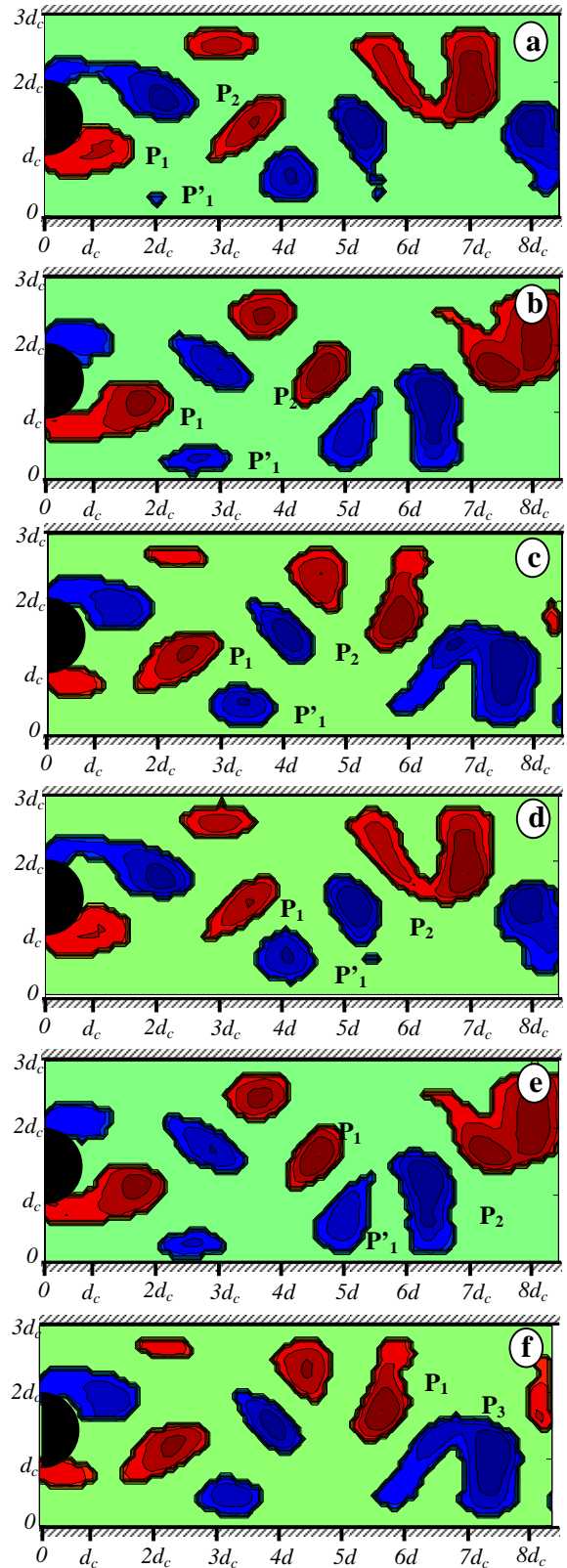


Figure 3: Coherent structures downstream the cylinder using Γ_2 criterion for $Re=159$ with a time step of $0.16 T$; from (a) to (f)

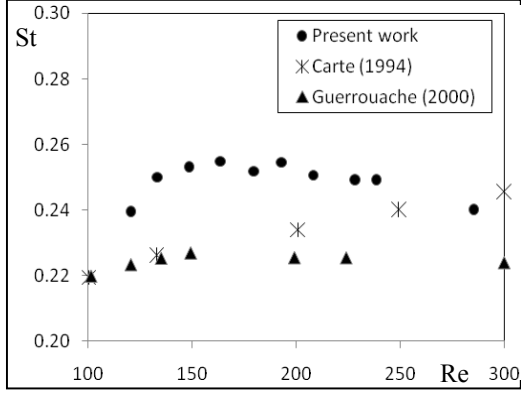


Figure 4. Evolution of the Strouhal number with Reynolds number

As the dynamic presents a symmetry axis $y = \frac{3}{2}d_c$, only what happening at the lower part of the tunnel is discussed. When the vortex (P_1) is created (Fig.3.a), the wall reacts at this vorticity increasing of the vortex (P_1) by creating the vortex (P'_1). Before the detachment of the vortex (P_1) from the lower part of the cylinder (Fig.3.a-c), its growing is accompanied by a growing of the vortex (P'_1). In a second phase, i.e. when the vortex (P_1) is detached from the lower part of the cylinder, the vortex (P'_1) remains coupled with (P_1) which is pushed far from the lower wall. The two vortices (P_1) and (P'_1) are advected downstream the cylinder. The vortex (P'_1) enter in coalescence with a vortex type (P_2) created before and detached from the upper part of the cylinder. The coalescence position depends on the Reynolds number and it is shown in the figures 3.e-f. This coalescence gives birth to a vortex (P_3) which rolls at the lower part of the cylinder. It is to be noticed that the same dynamic takes place at the lower part of the tunnel.

3.2 Coherent structures interaction with walls and their reorganization

As it was announced in the previous section, the creation of a von Kármán vortices P_i ($i \in \{1, 2\}$) behind the cylinder creates a reaction at wall which exhibit the appearance of a vortex with a opposite sign. This vortex called P'_i ($i \in \{1, 2\}$) grows with the growing of the von Kármán vortex and advected with the von Kármán vortex in the flow direction. Two essential parameters are used here to find a relationship between the cause and the consequence vortices which are the vortices circulations of and their respective local kinetic energies.

The circulation of a vortex is defined as:

$$Cir = \oint_{S_v} \vec{U} d\vec{l} = \iint_{S_v} \omega dS \quad (2)$$

where S_v is the instantaneous surface of the vortex.

The local kinetic energy of a vortex is defined as follows:

$$Ecl = \iint_{S_v} \left(\frac{1}{2} (\vec{U} - \vec{U}_{ad})^2 \right) dS \quad (3)$$

where \vec{U}_{ad} is the advection velocity of the vortex.

To calculate these two parameters, the first step consists in finding at first the instantaneous vortex limits (i.e.: surface) and the vortex center. The Γ_2 criterion defines the limit of a two dimensional vortex as the space region where $|\Gamma_2| > \frac{2}{\pi}$ and the vortex centre position as $max(|\Gamma_2|)$. Knowing the instantaneous positions of the vortex centre, the calculation of the instantaneous advection velocity of the vortex is consequent. The table 1 gives a recapitulative of the different advection velocities. We notice also that an alternative to calculate the advection velocity of a flow when its limits are well defined is as follows:

$$\vec{U}_{ad} = \frac{1}{S_v} \iint_{S_v} \vec{U}(x, y, t) dS \quad (4)$$

where S_v is the vortex surface.

Table 1: Advection velocities of the different vortices

Re	Vortex P_1 (mm/s)	Vortex P'_1 (mm/s)
129	Uadx = 11.2 Uady = -1.3	Uadx = 8.1 Uady = 1.1
159	Uadx = 13.4 Uady = -1.9	Uadx = 9.9 Uady = 1.2
188	Uadx = 15.6 Uady = -2.6	Uadx = 10.4 Uady = 1.9
233	Uadx = 19.2 Uady = -3.1	-----
277	Uadx = 20.5 Uady = -4.3	Uadx = 12.7 Uady = 2.2

This alternative is interesting when the advection velocity of the vortex is not constant.

When the vortex P_1 is generated at the lower part of the cylinder, its circulation grows linearly with the axial position of the vortex centre until its complete detachment downstream the cylinder (Fig.5.a).

After this step, the circulation of the vortex decreases exponentially with the axial position of the vortex centre, since its energy is attenuated under the high viscous effects in this region of the flow. The same remarks are also valid for the local kinetic energy of the vortex (Fig.5.b).

As the creation of the von Kármán vortices are the source of the appearance of the vortices P'_i at wall, it is interesting to find a relation between the different parameters concerning these two families of vortices. By calculating the ratio

$$\left| \frac{Cir(P'_1)}{Cir(P_1)} \right| = f(x_{P_1}),$$

it was found that this ratio is independent of the Reynolds number for the range of Reynolds studied (Fig.6.a.). It exhibits two evolutions. In the first phase, i.e. when the vortex P_1 is in the growing phase (phase 1), the ratio

$$\left| \frac{Cir(P'_1)}{Cir(P_1)} \right| = f(x_{P_1}) \approx 0.22 \mp 0.02$$

for all the Reynolds number range studied. In the second phase (phase 2), the circulation $|Cir(P_1)|$ decreases with x_{P_1} . At opposite, $|Cir(P'_1)|$ continues in increasing until a limit value that depends with the Reynolds number and the ratio

$$\left| \frac{Cir(P'_1)}{Cir(P_1)} \right| = f(x_{P_1})$$

is independent of the Reynolds number and it can be approached by a linear curve as:

$$\left| \frac{Cir(P'_1)}{Cir(P_1)} \right| = 0.38 \left(\frac{x_{P_1}}{d_c} \right) - 0.62 \quad (5)$$

A similar relationship between P_1 and P'_1 by considering their respective local kinetic energies $Ecl(P_1)$ and $Ecl(P'_1)$ (Fig.6.b). In fact, in the phase 1, the ratio remains constant with

$$\frac{Ecl(P'_1)}{Ecl(P_1)} \approx 0.05 \pm 0.005 \quad (6)$$

In the second phase, this ratio increases as a parabolic of x_{P_1} as:

$$\frac{Ecl(P'_1)}{Ecl(P_1)} \approx 0.132 \left(\frac{x_{P_1}}{d_c} \right)^2 - 0.43 \left(\frac{x_{P_1}}{d_c} \right) + 0.38 \quad (7)$$

Finally, one can notice that we can write for both phases:

$$\frac{Ecl(P'_1)}{Ecl(P_1)} = \left| \frac{Cir(P'_1)}{Cir(P_1)} \right|^2 \quad (8)$$

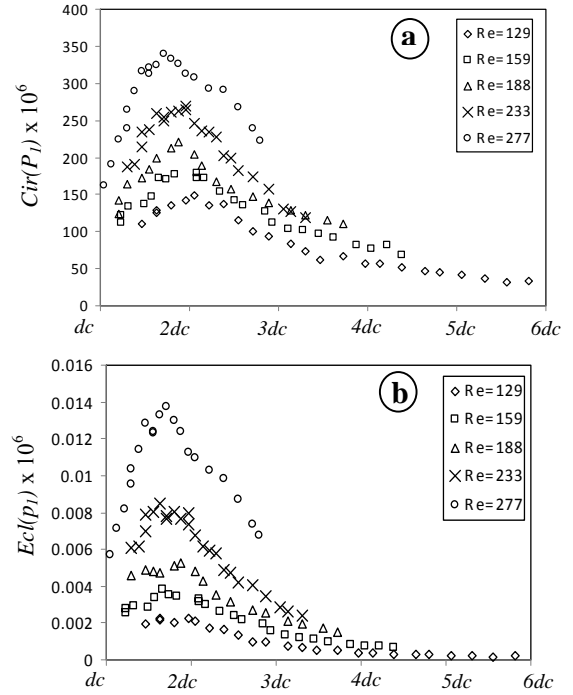


Figure 5: Evolution of the vortex with its center position for different Reynolds numbers:

- a) Circulation of the vortex;
- b) Local kinetic energy of the vortex

After the formation of the vortex P'_1 , it is advected downstream the cylinder and enter in coalescence with the vortex P_2 detached from the upper side of the cylinder. This coalescence takes place at a position x_{P_2} of the vortex P_2 that depends of the Reynolds number. It should be noticed that when the coalescence of P'_1 and P_2 takes place, the vortex P'_1 is absorbed by P_2 gradually and the new created vortex P_3 .

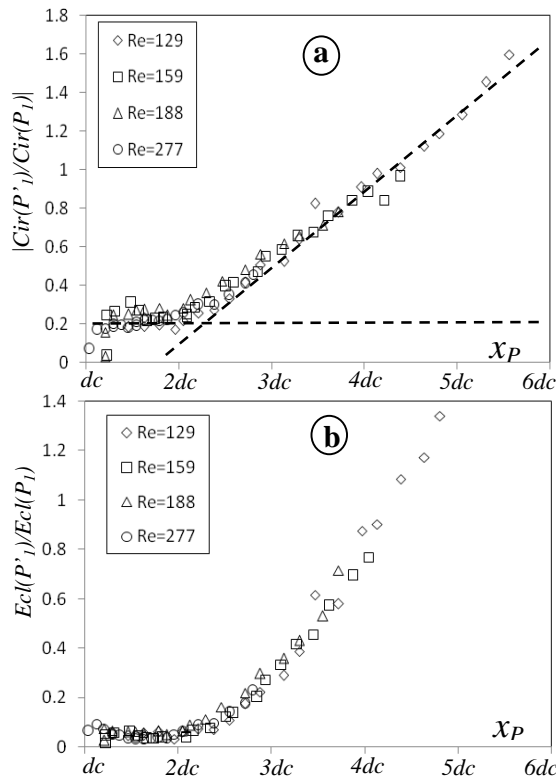


Figure 6: a) Evolution of the circulation ratio

$\frac{|Cir(P'_i)|}{|Cir(P_i)|}$ with the axial position of the vortex P_i ;

b) Relationship between the local kinetic energies of the vortices P_i and P'_i with x_{P_i}

4. CONCLUSION

In this work, we presented the interaction of a cylinder wake with two parallel walls. The experimental results exhibit that the interaction between a vortex and a wall is characterized by the creation of a secondary one at wall with an opposite vorticity sign. It was also found a relationship between the local kinetic energies and the circulation of the primary vortices (P_i) and the secondary ones (P'_i). These results have to be validated with other experimental or numerical simulations.

ACKNOWLEDGEMENTS

This research was supported by the laboratory GEPEA of the (university of Nantes, France), the laboratory LESTE (university of Monastir, Tunisia), and the CNRS (France). These supports are gratefully acknowledged.

REFERENCES

Carte G., Simulation d'écoulements instationnaires à dominante périodique. Application aux sillages laminaires turbulents, PhD Thesis, Université d'Aix-Marseille II, 1994.

Coutanceau M., Bouard R., Experimental determination of the main features of the viscous flow in the wake of a cylinder in uniform translation, Part 1: Steady flow, Journal of Fluid Mechanics, 79, 231-256, 1977.

Escriva X., Étude dynamique et thermique des transferts pariétaux instationnaires: Application à l'interaction tourbillon couche limite, PhD. Thesis, Université de Paul Sabatier, France, 1999.

Graftieaux L., Michard M., Grosjean N., Combining PIV, POD and vortex identification algorithms for the study of unsteady turbulent swirling flows, Measurements and Science Technology, 1422-1429, 2001.

Guerrouache M.S., Étude numérique de l'instabilité de Bénard-Kármán derrière un cylindre fixe ou en mouvement périodique, Dynamique de l'écoulement et advection chaotique, PhD. Thesis, Université de Nantes, 2000.

Natarajan N. M., Lakshmanan S.M., Laminar flow in rectangular ducts: prediction of velocity profiles and friction factor, Indian Journal of Technology, 435-438, 1972.

Rehimi F., Aloui F., Ben Nasrallah S., Doubriez L., Legrand J., Experimental investigation of the flow downstream a circular cylinder centered between two parallel walls, Journal of fluid and structures, vol. 24, No 6, 855-882, 2008.

Sahin, M., Owens, R.G.. A numerical investigation of wall effects up to high blockage ratios on two-dimensional flow past a confined circular cylinder. Physics of Fluids, 16, 1305-1320, 2004.

Williamson C.H.K., Defining a universal and continuous Strouhal-Reynolds number relationship for the laminar vortex shedding of a circular cylinder at low Reynolds number, Phys. Fluids, 31, 2742, 1989.

Williamson C. H. K., Three-dimensional vortex dynamics in bluff body wakes, Experimental Thermal and Fluid Science, Vol. 12, pp 150-168, 1996.

Yang Y., Shehata A., Modi V. , West A. C., Mass transfer to a channel wall downstream of a cylinder, Int. J. Heat Mass Trans., Vol. 40, 4263-4271, 1997.

Zovatto L., Pedrizzetti G., Flow about a circular cylinder between parallel walls, Journal of Fluid Mechanics 440, 1-25, 2001.